Desalination and Water Treatment
www.deswater.com

doi:10.5004/dwt.2018.22745

120 (2018) 248–260
July

Synthesis and characterization of graphene oxide nanosheets decorated with Fe_3O_4 nanoparticles: an efficient adsorbent for nickel(II) removal

Xue Li[a,b], Kang Zhao[a,*], Caiyin You[a,*], Wensheng Linghu[c], Mei Yu[d], Ahmed Alsaedi[e], Tasawar Hayat[e,f], Hui Pan[b], Jie Luo[b]

[a]*School of Materials Science and Engineering, Xi'an University of Technology, Xi'an 710048, P.R. China, email: 81850609@qq.com, lixue.213@usx.edu.cn (X. Li), Tel./Fax +86 29 82312799, email: kzhao@xaut.edu.cn (K. Zhao), caiyinyou@xaut.edu.cn (C. You)*
[b]*College of Yuanpei, Shaoxing University, Shaoxing 312000, P.R. China, email: panhui33@163.com (H. Pan), tangxp@usx.edu.cn (X. Tang), lj26wlxy@163.com(J. Luo)*
[c]*College of Chemistry and Chemical Engineering, Shaoxing University, Shaoxing 312000, P.R. China, email: wslinghu@usx.edu.cn (W. Linghu)*
[d]*Department of Physics, Shaoxing University, Shaoxing 312000, P.R. China, email: 1688465@qq.com (M. Yu)*
[e]*NAAM Research Group, Department of Mathematics, Faculty of Science, King Abdulaziz University, Jeddah 21589, Saudi Arabia, email: aalsaedi@hotmail.com (A. Alsaedi), fmgpak@gmail.com (T. Hayat)*
[f]*Department of Mathematics, Quaid-I-Azam University, Islamabad 44000, Pakistan*

Received 3 December 2017; Accepted 8 July 2018

ABSTRACT

In this work,we synthesized and characterized the magnetic graphene oxide (MGO) composite, and used it for the removal of Ni(II) from aqueous solutions as a high efficient and low-risk adsorbent. The results showed that the adsorption of Ni(II) on MGO is endothermic and spontaneous. The absorption of Ni(II) on MGO is strongly dependent on pH values due to the electrostatic interaction. The adsorption kinetic and isotherms were fitted the pseudo-second-order and Langmuir model well, respectively. The results also indicated that the combination of the excellent adsorption capacity of GO and the magnetic properties of Fe_3O_4 is extremely valuable, which has a good application prospect due to it has many advantages such as easy magnetic separation, excellent repeat-ability and environment-friend.

Keywords: Adsorption; Isotherm; Kinetics; Magnetic graphene oxide; Ni(II)

1. Introduction

The presence of hazardous contaminants in water is an important issue in environmental pollution management due to their hazards on human health [1–12]. Nickel is a kind of non-biodegradable toxic heavy metal in wastewater. Its concentration increases in the water system due to the various engineering processes such as galvanizing, smelting, mining, battery, and metal finishing, resulting in toxic and carcinogenic effect on living species [13,14]. The tolerance limit of nickel in drinking water is 1.7×10^{-7} mol L^{-1}, and for industrial wastewater it is 3.4×10^{-5}mol L^{-1} [15]. However, effluents of different industries contain higher concentration of nickel than its acceptable limit. Thereby, it is very important to remove nickel from wastewater. Many technologies such as ion exchange, coagulation/coprecipitation, membrane filtration, precipitation, electrochemical, filtration and reverse osmosis have been proposed by different scientific workers for the removal of nickel from aqueous solution and effluents [15]. However, most of these technologies require high operational and maintenance costs, and also cause secondary pollution [16,17]. As an economical

*Corresponding author.

and efficient method, adsorption technique has been widely applied to remove heavy metals from wastewaters. Therefore, a large number of adsorbents, such as graphene/δ-MnO_2 (42.85 mg g^{-1}) [18], diatomite [19,20], mordenite [21], Na-attapulgite (6.16 mg g^{-1}) [22], Na-rectorite (10.21 mg g^{-1}) [23], GMZ bentonite (14.61 mg g^{-1}) [24], titanate nanotubes [25], carbon nanotube (3.88 mg g^{-1}) [26] have been reported as potential adsorbents for nickel ion removal from aqueous solutions. However, the application on a large scale in the practical applications of Ni(II)removal for these adsorbents are limited for their low adsorption capacities and it is difficult to separate the adsorbents from aqueous solutions. Therefore, in order to address these issues, it is of significant importance for researchers to still make great efforts to investigate new adsorbents with higher adsorption capacities and the advantage of easy separation from solutions.

Graphene oxide (GO), one of the most important derivatives of graphene, are extensively investigated due to high surface area, high electro-/thermoconductivities, high chemical/electrochemical stability, and high flexibility and elasticity. GO has the sufficient quantity of oxygenous functional groups (epoxy, hydroxyl, and carboxyl groups) and high water solubility serve GO sheets great promise as an ideal adsorbent of metal oxides [27–29]. In comparison to other carbonaceous nanomaterials, GO may be more environmental friendly and have better biocompatibility [30]. Therefore, various multifunctional hybrid materials based on graphene have been synthesized using GO and applied for the removal of various heavy metal ions and organic pollutants [31–38]. However, it is difficult to separate GO from aqueous solution using traditional centrifugation and filtration methods during and after the adsorption process due to its small particle size [39,40]. Fortunately, the introduction of magnetic materials into GO can combine the high adsorption capacity of GO and the separation convenience of magnetic materials, which have been used in the field of environmental remediation recently. For example, Zhao et al. [39] investigated the preparation of amino functionalized graphene oxide decorated with Fe_3O_4 nanoparticles for the adsorption of Cr(VI), Shenget al. [27] studied the removal of arsenate by versatile magnetic graphene oxide composites. Li et al. [41] synthesized magnetic graphene composites for Cd(II) removal. However, to the best of our knowledge, the limited information about the adsorption performance and mechanism of graphene-based magnetic composites towards inorganic and organic contaminants severely limits its practical application in environmental pollution management. Therefore, investigating the thermodynamics and kinetics of Ni(II) adsorption on graphene oxide nanosheets decorated with Fe_3O_4 nanoparticles are imperative.

The objective of this paper focused on highly efficient removal of Ni(II) using graphene oxide nanosheets decorated with Fe_3O_4 nanoparticles. In the previous work, (1) the magnetic graphene oxide (MGO) composites were synthesized and applied to the removal of Ni(II) from aqueous solutions by batch experiments, (2) the characterization of MGO composite was described to evaluate the synthetic effectiveness, (3) to investigate the kinetic, thermodynamic and equilibrium models of Ni(II) removal by MGO composite, (4) to study the effect of pH on Ni(II) adsorption, and (5) to discuss the interaction mechanism of Ni(II) with MGO under different experimental conditions. The present study is an extension of our research on the possible use of GO-based nanocomposites as versatile adsorbents for metals removal in environmental pollution cleanup.

2. Experimental section

2.1 Materials and preparation of MGO composites

Graphite powder (99.95% purity, average diameter of 20 mm, Qingdao Graphite Company, China), Ni metal powder (99.9%purity), $KMnO_4$, $FeCl_3{\cdot}6H_2O$, $FeCl_2{\cdot}4H_2O$, ammonia solution, H_2SO_4 (98%), H_2O_2 (30%), glycol and all other reagents in analytical purity used in the experiments were purchased from Sinopharm Chemical Reagent Co. Ltd. and without any purification. All solutions were prepared and rinsed with Milli-Q water.

GO was prepared by using the modified Hummers method from the flake graphite,and the characterization of GO had been reported in our previous study in detail [42,43]. The GO/Fe_3O_4 composites was synthesized by coprecipitation of $FeCl_3{\cdot}6H_2O$ and $FeCl_2{\cdot}4H_2O$ in the GO suspension about at 80°C under N_2. Briefly, the appropriate amount of $FeCl_3{\cdot}6H_2O$ and $FeCl_2{\cdot}4H_2O$ were mixed and added slowly to the GO suspension, then, the ammonia solution was added quickly to the above suspension for synthesis of magnetite particles (Fe_3O_4) while the temperature was raised to 85°C, and a 30% ammonia solution was added to adjust the pH to 10. After, the solution was cooled to room temperature meanwhile accompany rapidly stirred for 1 h. Then, the dark-black colored solution was filtered and washed with Milli-Q water/ethanol and dried in a vacuum at 70°C, thus, the GO/Fe_3O_4composites were prepared, and then stored in desiccator for further experiments. Fe_3O_4 was prepared by the same chemical coprecipitation method without GO [44].The detailed characterization of these materials are shown in the supporting information (SI).

2.2 Batch adsorption experiments

For Ni(II) adsorption, at first, Ni(II) stock solution was prepared by dissolving Ni metal powder in 10 mL of 3 M HNO_3 and then transferred into a 100 mL vessel. The stock solution was diluted with Milli-Q water to obtain standard solutions with concentrations ranging from 3.4×10^{-5} to 2.7×10^{-4} mol L^{-1}. MGO, GO or Fe_3O_4 stock suspensions were prepared by ultrasonication of MGO in Milli-Q water to achieve the concentration of 1.7×10^{-3} mol L^{-1}, and was severely shaken to obtain a homogeneous suspension. Then, sorption of Ni(II) on MGO, GO or Fe_3O_4 was carried out by batch sorption technique in a 10 mL polyethylene centrifuge tube, where a stock suspension of the MGO, GO or Fe_3O_4 and stock solutions of $NaNO_3$ and Ni(II) were added to achieve the desired concentrations of the different components [27,44]. The system was adjusted to the desired pH by adding negligible volumes of 0.01 or 0.1 mol L^{-1} NaOH or HNO_3. After the mixture was oscillated for 24 h to achieve complete equilibrium, the solid and liquid were separated by the magnetic separation method. Final, The concentration of Ni(II) was analyzed by spectrophotometer at wavelength 530 nm through the formation of Ni butane-

dione dioxime complex. The adsorption percentage (%) of Ni(II) from aqueous solution was calculated as [45–49]:

$$R(\%) = ((C_0 - C_e / C_0)) \times 100\% \quad (1)$$

where C_0 (mol L^{-1}) is the initial concentration of Ni(II) in suspension, C_e (mol L^{-1}) is the concentration in supernatant after centrifugation, respectively. The amounts of Ni(II) adsorbed on MGO, GO or Fe_3O_4 (q_e) are calculated from the following equations [45–49]:

$$q_e = (C_0 - C_e)V / m \quad (2)$$

where q_e (mol L^{-1}) is the concentration of Ni(II) adsorbed on MGO, GO or Fe_3O_4, m (g) is the mass of adsorbent, and V is the volume of the suspension. And the distribution coefficient (K_d) are calculated from the equations [45–49]:

$$K_d = (C_0 - C_e)V / mC_e \quad (3)$$

To confirm the experimental repeatability and improve data accuracy, the batch experiments were conducted in duplicate. The relative errors of the experimental data were less than 5%.

3. Results and discussion

3.1. Effect of contact time

As can be found Fig. 1, the adsorption rate of Ni(II) adsorption to MGO is fast at pH = 5.0 and 6.5, which owing to the laminated structure and large external surface of MGO. The adsorption process can be divided into two stages: (a) a rapid uptake within the first 2.5 h of contact time, in which ~40% of Ni(II) was removed at pH = 5.0 and ~ 26% of Ni(II) was removed at pH = 6.5; and (b) a slow uptake thereafter until an equilibrium was reached [50–54].

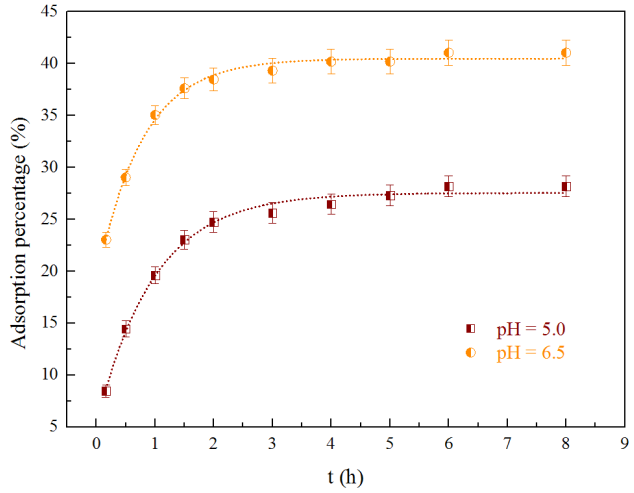

Fig. 1. Adsorption of Ni(II) on MGO as a function of contact time, T = 303 K, I = 0.01 mol·L^{-1} $NaNO_3$, C $(Ni(II))_{initial}$ = 2.6 × 10^{-4} mol·L^{-1}, m/V = 1.7 × 10^{-3} mol·L^{-1}.

According to these results, 18 h was selected as the shaking time to ensure the full equilibrium in the following experiments.

3.2. Kinetic studies

In order to understand the adsorption property of Ni(II) on MGO and explain to the mechanism of the adsorption processes, the kinetics of Ni(II) adsorption on MGO was further analyzed and studied in terms of six kinetic models which have been widely used to fit the kinetic process of metal ion adsorption at the solid/water interfaces. These kinetic models are pseudo-first-order kinetic model, pseudo-second-order kinetic model, Elovich model, Intraparticle diffusion equation, Bangham model and Liquid film diffusion model, respectively. The curves fitted by these six kinetic models are shown in Fig. 2 and the relative adsorption parameters calculated from these models are listed in Table 1.

The pseudo-first-order kinetic model is generally expressed as [55]:

$$\ln(q_e - q_t) = \ln q_e - K_1 t \quad (4)$$

where q_t (mg g^{-1}) is the amounts of Ni(II) adsorbed at contact time t (h) and q_e (mg g^{-1}) is the adsorption amount at equilibrium time, respectively. K_1 (g mg^{-1} h^{-1}) is the pseudo-first-order kinetic model constant. The values of q_e can be calculated from the intercept and slope of the plot of $-\ln(q_e - q_t)$ vs. t (Fig. 2A) are 13.98 mg g^{-1} at pH = 5.0 and 10.67 mg g^{-1} at pH = 6.5, respectively. These values is not consistent with the experimental data and the correlation coefficient (R^2) is far away from 1.0. By this token, the pseudo-first-order kinetic model can't be used to fit the experimental data of Ni(II) adsorption on MGO.

The pseudo-second-order kinetic model is generally expressed as [56]:

$$t / q_t = 1 / K_2 \times q_e^2 \quad (5)$$

where K_2 (g mg^{-1} h^{-1}) is the pseudo-second-order kinetic model constant. The values of q_e can be calculated from the intercept and slope of the plot of t/q_t vs. t (Fig. 2B) are 30.00 mg g^{-1} at pH = 5.0 and 42.02 mg g^{-1} at pH = 6.5, respectively. These values is consistent with the experimental data and the correlation coefficient (R^2) is nearly close to 1.0. The pseudo-second-order kinetic model fitted well with the experimental data as can be seen Fig. 2B. These characteristics suggest that the kinetic adsorption of Ni(II) on MGO follows the pseudo-second-order kinetic model very well.

The elovich model is generally expressed as [57]:

$$q_t = \frac{1}{\beta}\ln(\alpha - \beta) + \frac{1}{\beta} lnt \quad (6)$$

where α (mg g^{-1} h^{-1}) is the initial adsorption rate, β (g mg^{-1}) is the elovich model desorption constant, respectively. The curves fitted by plot of q_t vs. ln$t$ is shown in Fig. 2C. The correlation coefficient (R^2) is 0.9592 or 0.9204, which better than the pseudo-first-order kinetic model, worse than the pseudo-second-order kinetic model.

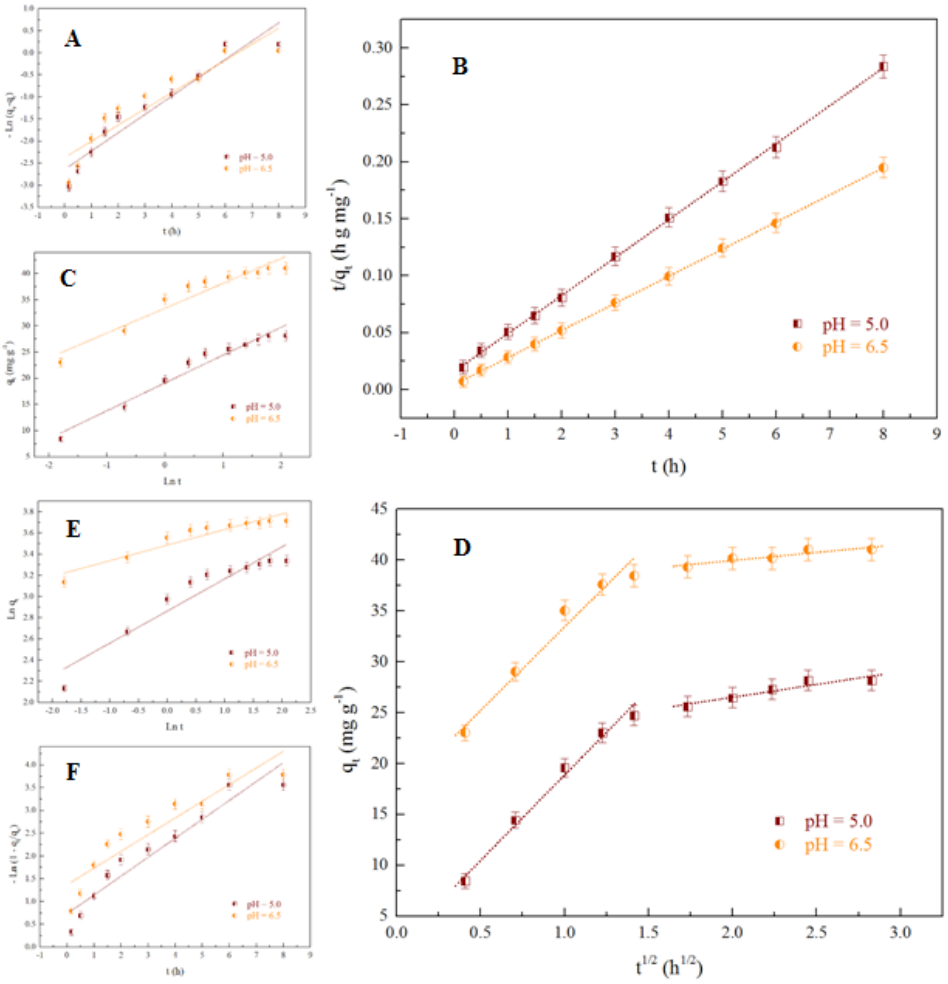

Fig. 2. The kinetic model fitting of Ni(II) on MGO, T = 303 K, I = 0.01 mol·L^{-1} $NaNO_3$, C (Ni(II))$_{initial}$ = 2.6 × 10^{-4} mol·L^{-1}, m/V = 1.7 × 10^{-3} mol·L^{-1}. (A) The pseudo-first-order kinetic model, (B) The pseudo-second-order kinetic model, (C) Elovich model, (D) Intraparticle diffusion model, (E) Bangham model and (F) Liquid film diffusion model.

The intraparticle diffusion model is generally expressed as [57]:

$$q_t = K_{id} t^{1/2} + C \tag{7}$$

where K_{id} (mg g^{-1} h$^{-0.5}$) is indicative of the intraparticle diffusion model constant, and C (mg g^{-1}) is indicative of the intercept of the line. The curves fitted by plot of q_t vs. $t^{1/2}$ is shown in Fig. 2D. The correlation coefficient (R^2) suggests that the intraparticle diffusion model can be used to fit the experimental data of Ni(II) adsorption on MGO. According to this model, the plot linearity suggests that intra-particle diffusion also affects the adsorption rate.

The bangham model is generally expressed as [57]:

$$\ln q_t = \ln K_b + (1/m)\ln t \tag{8}$$

where K_b (mg g^{-1}) and m (g mg^{-1} h^{-1}) is indicative of the bangham model constant. The curves fitted by plot of ln q_t vs. ln t is shown in Fig. 2E. The correlation coefficient (R^2) is far away from 1.0 suggests that the bangham model can't be used to fit the experimental data of Ni(II) adsorption on MGO.

The liquid film diffusion model is generally expressed as:

$$\ln(1 - q_t / q_e) = -K_{fd} t \tag{9}$$

where q_t/q_e is the function attainment of sorption equilibrium and K_{fd} (h^{-1}) is indicative of the liquid film diffusion model constant. The curves fitted by plot of $-\ln(1 - q_t/q_e)$ vs. t is shown in Fig. 2F. The correlation coefficient (R^2) is far away from 1.0 suggests that the liquid film diffusion model can't be used to fit the experimental data of Ni(II) adsorption on MGO.

3.3. Adsorption isotherms

To evaluate the interaction between an adsorbate and an adsorbent and to design and operate an adsorption system successfully, equilibrium adsorption isotherm data is very important. To evaluate the adsorption capacity of the

Table 1
Kinetic parameters of Ni(II) adsorption on MGO

pH	Pseudo first order parameters		
	q_e (mg·g^{-1})	K_1 (g·mg^{-1}·h^{-1})	R^2
5.0	13.98	0.41	0.8161
6.5	10.68	0.37	0.7444
pH	Pseudo second order parameters		
	q_e (mg·g^{-1})	K_2 (g·mg^{-1}·h^{-1})	R^2
5.0	30.00	3.46 × 10^{-2}	0.9995
6.5	42.02	6.38 × 10^{-2}	0.9999
pH	Elovich model parameters		
	α (mg g^{-1} h^{-1})	β (g mg^{-1})	R^2
5.0	36.59	0.12	0.9592
6.5	1141.48	0.21	0.9204
pH	Intra particle diffusion model parameters		
	C (mg g^{-1})	K_{id} (mg g^{-1} h$^{-0.5}$)	R^2
5.0	10.56	7.53	0.9856
6.5	26.02	6.55	0.9591
pH	Bangham model parameters		
	m (g mg^{-1} h^{-1})	K_b (mg g^{-1})	R^2
5.0	3.30	17.53	0.7982
6.5	6.79	32.65	0.7883
pH	Liquid film diffusion model parameters		
	Intercept	K_{fd} (h^{-1})	R^2
5.0	0.73	0.41	0.8161
6.5	1.37	0.37	0.7444

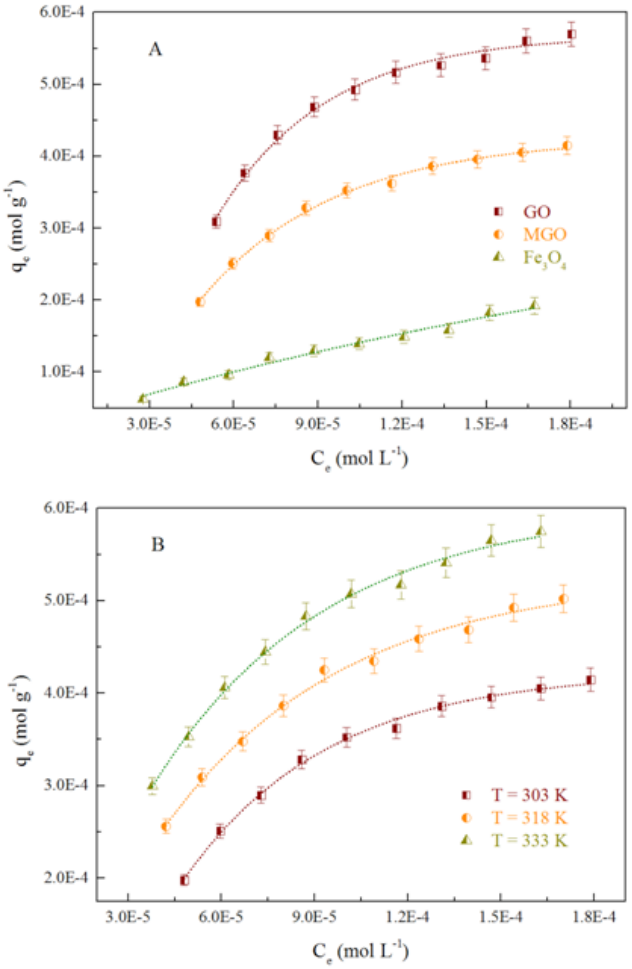

Fig. 3. (A) The adsorption isotherms of Ni(II) on GO, MGO and Fe_3O_4, T = 303 K, pH = 5.0, I = 0.01 mol·L^{-1} $NaNO_3$, m/V = 1.7 × 10^{-3} mol·L^{-1}; (B) The adsorption isotherms of Ni(II) on MGO at three different temperatures, pH = 5.0 ± 0.1, I = 0.01 mol·L^{-1} $NaNO_3$, m/V = 1.7 × 10^{-3} mol·L^{-1}.

as-prepared adsorbents, the adsorption of Ni(II) on Fe_3O_4, GO and MGO was studied. It can be clearly seen from Fig. 3A that the adsorption isotherm keeps raising under our experimental conditions. Although the q_e value of Ni(II) on MGO is lower compared to that of Ni(II) on GO, which is caused by the reduction of the effective adsorbing sites after combination of Fe_3O_4 on GO. However, the GO nanoparticles cannot be separated from solution easily, but the MGO can be easily separated from solution by inducing an external magnetic field. Therefore, this is worthwhile that sacrificing a small amount of adsorption to facilitate separation.

The equilibrium adsorption isotherm plays a very important role for the determination of adsorption mechanism. The adsorption isotherms for Ni(II) on MGO at three different temperatures (303, 318 and 333 K) are analyzed and shown in Fig. 3B. The adsorption isotherm is the highest at T = 333 K and is the lowest at T = 303 K, which suggesting that Ni(II) adsorption on MGO is favored at higher temperatures. In order to simulate and understand the adsorption mechanism by analyze the experimental equilibrium adsorption data in the present work, five typical isotherm models, such as Linear, Langmuir, Freundlich, Dubinin-Radushkevitch (D-R) and Temkin adsorption isotherm model are used to describe the equilibrium data.

The Linear model can be represented as:

$$q_e = A + BC_e \tag{10}$$

where A and B are the Linear constants. The Langmuir model can be represented as:

$$C_e / q_e = \left(1/b + C_e\right) / q_{\max} \tag{11}$$

where q_{max} (mol g^{-1}) and b (L mol^{-1}) are the Langmuir constants, which are related to adsorption capacity and adsorption energy, respectively. The Freundlich model can be represented as:

$$\log q_e = \log K_F + n \log C_e \tag{12}$$

where K_F (mol^{1-n} L^n g^{-1}) and n are the Freundlich constants, K_F represents adsorption capacity and n represents the degree of dependence of adsorption at the equilibrium concentration. The D-R model can be represented as:

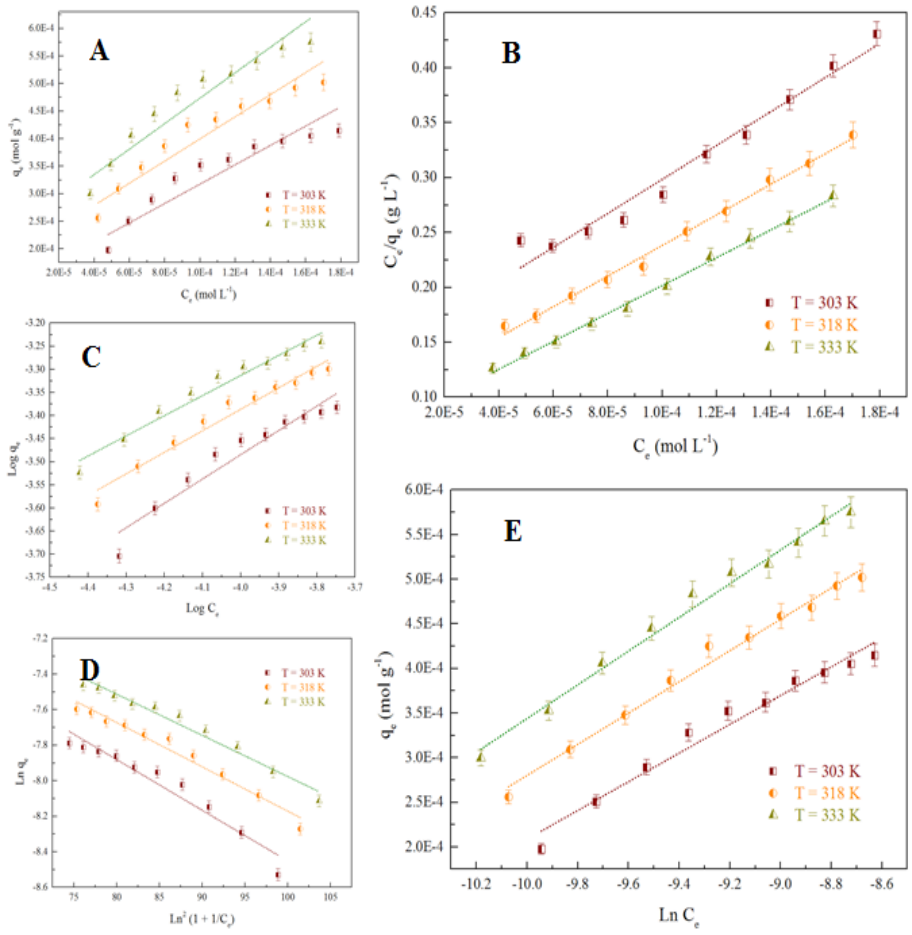

Fig. 4. The fitting results of (A) Linear, (B) Langmuir, (C) Freundlich, (D) D-R and (E) Temkin adsorption isotherms of Ni(II) adsorption on MGO at three different temperatures, pH = 5.0 ± 0.1, I = 0.01 mol·L^{-1} $NaNO_3$, m/V = 1.7 × 10^{-3} mol·L^{-1}.

$$\ln q_e = \ln q_{\max} - \beta\varepsilon^2 \tag{13}$$

where β (mol^2 kJ^{-2}) is the D-R activity constant, and ε is the Polanyi potential, which is equal to

$$\varepsilon = RT\ln\left(1+1/C_e\right) \tag{14}$$

where R (8.3145 J mol^{-1} K^{-1}) is ideal gas constant , and T(K) is the absolute temperature in Kelvin, E (kJ mol^{-1}) is defined as the free energy change, its value $E = 1/\sqrt{2\beta}$. The Temkin model can be represented as:

$$q_e = B_1 \ln K_T + B_1 \ln C_e \tag{15}$$

where K_T (mol L^{-1}) and B_1 are the Temkin constants [58].

The curves fitted by these five isotherm models are shown in Fig. 4 and the relative isotherm parameters calculated from these models are listed in Table 2. By comparing the regression correlation coefficients (R^2) and fitting curves shown in Fig. 4, it is obvious that the Langmuir model fits the experimental data is best in these five isotherm models, followed by Temkin model. The fact that the sorption data of Ni(II) is in accordance with the Langmuir model suggests that the adsorbed with homogeneous binding sites, equivalent adsorption energies, no interaction between adsorbed species, and monolayer coverage is the main sorption mechanism of Ni(II) adsorption on MGO [59]. The values of q_{max} calculated from the Langmuir model are the lowest (26.37 mg g^{-1}) at T = 303 K and the highest (34.69 mg g^{-1})at T = 333 K, which indicates that the sorption is improved with increasing temperature.

3.4. Thermodynamic studies

In order to investigate the thermodynamic properties of Ni(II) adsorption onto MGO, the thermodynamic parameters (including the Gibbs free energy ΔG^0, entropy ΔS^0, and enthalpy ΔH^0) can be determined from the temperature dependence adsorption isotherms. The ΔG^0 values can be calculated by the relationship:

$$\Delta G^0 = -RT\ln K^0 \tag{16}$$

where K^0 is adsorption equilibrium constant. The values of $\ln K_d^0$ can be obtained by plotting $\ln K_d$ versus C_e for Ni(II) adsorption onto MGO and extrapolating C_e to zero (Fig. 5A), of which the intercept of the vertical axis gives

Table 2
The parameters for Linear, Langmuir, Freundlich, D–R and Temkin isotherms of Ni(II) adsorption on MGO at different temperatures

Linear model	A	B		R^2
T = 303 K	1.41×10^{-4}	1.76		0.8846
T = 318 K	1.99×10^{-4}	2.01		0.9171
T = 333 K	2.42×10^{-4}	2.31		0.9158
Langmuir model	q_{max} (mol g^{-1})	b (L mol^{-1})		R^2
T = 303 K	4.47×10^{-4}	1.08×10^{-4}		0.9871
T = 318 K	5.17×10^{-4}	1.41×10^{-4}		0.9936
T = 333 K	5.88×10^{-4}	1.70×10^{-4}		0.9964
Freundlich model	K_F ($mol^{1-n}L^n$ g^{-1})	n		R^2
T = 303 K	4.16×10^{-4}	0.53		0.9223
T = 318 K	2.98×10^{-4}	0.47		0.9599
T = 333 K	2.68×10^{-4}	0.44		0.9636
D-R model	q_{max} (mol g^{-1})	β (mol^2 kJ^{-2})	E (kJ mol^{-1})	R^2
T = 303 K	3.70×10^{-3}	4.49×10^{-3}	10.55	0.9330
T = 318 K	3.42×10^{-3}	3.57×10^{-3}	11.84	0.9678
T = 333 K	3.48×10^{-3}	3.02×10^{-3}	12.86	0.9714
Tekin model	B_1	K_T (g L^{-1})		R^2
T = 303 K	1.61×10^{-4}	0.82×10^5		0.9680
T = 318 K	1.75×10^{-4}	1.09×10^5		0.9864
T = 333 K	1.89×10^{-4}	1.35×10^5		0.9881

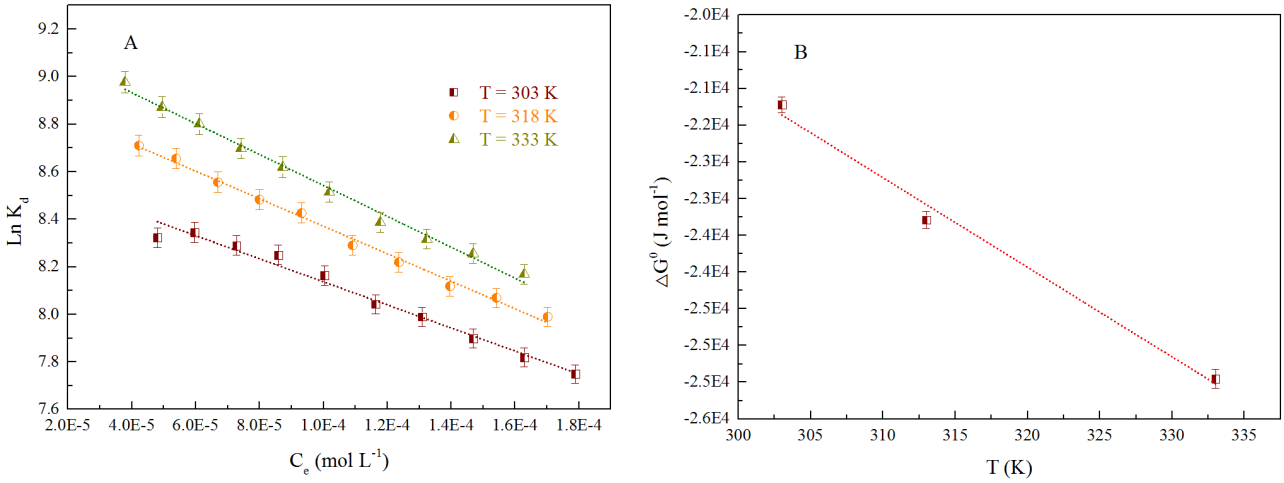

Fig. 5. (A) The linear plot of Ln K_d versus C_e at three different temperatures and (B) ΔG^0 versus T for Ni(II) adsorption on MGO, pH = 5.0 ± 0.1, I = 0.01 mol·L^{-1} $NaNO_3$, $m/V = 1.7 \times 10^{-3}$ mol·L^{-1}.

the value of lnK^0, are 8.62 (T = 303 K), 8.95 (T = 318 K) and 9.19 (T = 333 K), respectively. The ΔS^0 evaluated from the slope which linear plot of ΔG^0 versus T (Fig. 5B) is achieved according to the equation:

$$\left(\partial \Delta G^0 / \partial T\right)_P = -\Delta S^0 \tag{17}$$

and then the ΔH^0 is calculated from the expression as:

$$\Delta H^0 = \Delta G^0 + T\Delta S^0 \tag{18}$$

The determination of thermodynamic parameters provides a mechanism insight into Ni(II) adsorption on MGO and the values obtained are tabulated in Table 3. The positive value of ΔH^0 confirm an endothermic nature of adsorption of Ni(II) uptake on MGO, which is an indication of the existence of a strong interaction between Ni(II) and MGO. One possible explanation to this positive ΔH^0 is that Ni(II) ions are firstly to be stripped out (at least partially) of their hydration shell in the aqueous solutions, namely this process requires energy input. So, it is favored at high temperature. The positive value of ΔS^0 reflect an

Table 3
Values of thermodynamic parameters for Ni(II) adsorption on MGO

T(K)	ΔG^0 (kJ mol^{-1})	ΔS^0 (J mol^{-1}K^{-1})	ΔH^0 (kJ mol^{-1})
303	–21.72	121.99	17.97
318	–23.66		17.99
333	–25.45		18.17

increase in the randomness of the MGO-solution interfacial system during the uptake of Ni(II) on MGO, which implies some structural changes in Ni(II) and MGO during the uptake process. The ΔG^0 is negative as expected for a spontaneous process and feasible trend under the conditions applied. The value of ΔG^0 becomes more negative at 333 K suggested the more energetic favorable adsorption at higher temperature, because of a greater driving force of adsorption. The thermodynamic analysis derived from adsorption isotherms at three different temperatures suggests that the uptake process of Ni(II) on MGO is spontaneous and endothermic.

3.5. pH impact on Ni(II) adsorption

The pH of the aqueous solution is one of the most important parameters for metal adsorption. Therefore, a variation in pH can affect the kinetics and equilibrium characteristics of the adsorption process. The effect of the pH on theNi(II) adsorption on the MGO was studied and showed Fig. 6. As shown in Fig. 6, it is evident that the adsorption capacity of Ni(II) on MGO was highly dependent on the pH, which increases from 19 mg g^{-1} to 117 mg g^{-1} (removal percentage from 13% increases to 78%) with an increase in pH of the solution from 2.0 to 10.0 and then maintains high adsorption levels. In previous investigations, Hu et al. [4] studied the impact of pH on the sorption of Ni(II) from to goethite. Ren et al. [13] studied the impact of pH on the sorption of Ni(II) on Na-rectorite. Sheng et al. [19,20] studied the impact of pH on the sorption of Ni(II) on diatomite. Yang et al. [21,24] studied the impact of pH on the sorption of Ni(II) on mordenite and GMZ bentonite. Fan et al. [22] studied the impact of pH on the sorption of Ni(II) on Na-attapulgite. Yu et al. [60] studied the impact of pH on the sorption of Ni(II) on Na-montmorillonite. And similar results have been reported.

Generally, the electrostatic attraction or repulsion interaction of Ni(II) species with the MGO surface is main governing factor of controlling the Ni(II) adsorption on MGO. The speciation of Ni in aqueous solution is strongly pH-dependent and the major Ni(II) species in different pH ranges are also shown in Fig. 6. It is clear that Ni(II) presents in the species of Ni^{2+}, $Ni(OH)^+$, $Ni(OH)_2^0$, $Ni(OH)_3^-$, and $Ni(OH)_4^{2-}$ as a function of pH [42]. One can see from-Fig. 6 that the main specie is Ni^{2+} at pH < 9.5 approximately, while the Ni(II) ions are adsorbed to MGO has reached the maximum value. So, the discussion of Ni(II) adsorption on the MGO is not affected by precipitation. Besides, it is well known that a solid surface is positively charged at pH < pH_{ZPC} and negatively charged at pH > pH_{ZPC}, the point of zero charge (pH_{pzc}) of MGO was measured to be at pH ~ 4.62 [27,44].

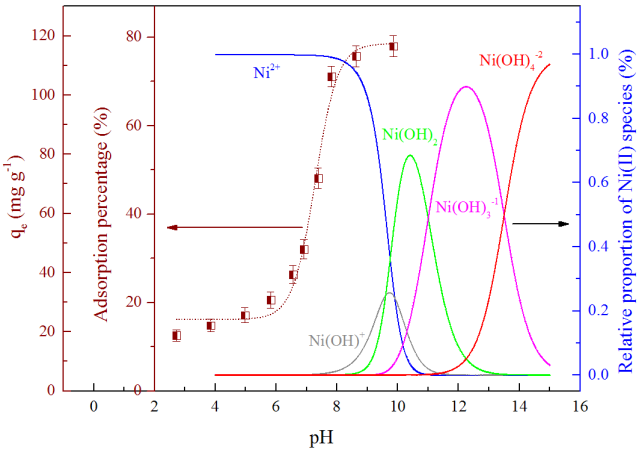

Fig. 6. The impact of pH on Ni(II) adsorption on MGO (T = 303 K, C (Ni(II))$_{initial}$ = 2.6 × 10^{-4} mol·L^{-1}, m/V = 1.7 × 10^{-3} mol·L^{-1}, I = 0.01 mol·L^{-1} $NaNO_3$) and relative proportion of Ni species as a function of pH.

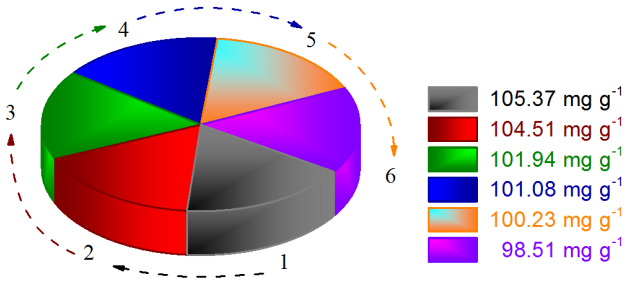

Fig. 7. Recycling for Ni(II) adsorption on MGO, T = 303 K, pH = 8.0 ± 0.1, C (Ni(II))$_{initial}$ = 2.6 × 10^{-4} mol·L^{-1}, m/V = 1.7 × 10^{-3} mol·L^{-1}, I = 0.1 mol·L^{-1} $NaNO_3$.

In addition, the MGO surface can become positively-charged as a result of protonation reaction (i.e., $SOH + H^+ \leftrightarrow SOH_2$) at low pH, the electrostatic repulsion occurred between Ni(II) and the positively-charged sites (MOH_2^+) on MGO results in the low uptake of Ni(II), which is partly attributed to the competition between H^+/Na^+ and Ni^{2+} on GO surface binding sites. In contrast, the MGO surface becomes negatively-charged due to the deprotonation process (i.e., $SOH + H^+ \leftrightarrow SOH_2$) and electrostatic repulsion obviously decreases with pH raising at high pH, which enhances the uptake of Ni(II) onto MGO through electrostatic force of attraction.

3.6. Regeneration study

As more and more metal ions are released into the natural water, it is very important to find a suitable material to treat the wastewater contaminated by metal ions [61–68]. The material of excellent-repeatability and environment-friend is a promising material in environmental remediation of metal-contaminated wastewater. For the environmental sustainability of MGO, the recycling of MGO in the removal of Ni(II) was investigated and the results are shown in Fig. 7. After adsorption, desorption was carried

out by washing out MGO bound Ni(II) with HNO_3 and by rinsing MGO with Milli-Q water; then, MGO was dried at 95°C and reused. From Fig. 7, this trend is very clear that the uptake capacity of Ni(II) onto MGO only showed a weak attenuation and the decline in efficiency is not more than 7% after recycle for six times. The results suggested that the MGO has a high repeatability which would add great value in the environmental pollution remediation, and indicated that MGO is a promising candidate for the removal of Ni(II) and related metal ions from aqueous solution.

4. Conclusions

In summary, MGO has been prepared to effectively remove Ni(II) from aqueous solution. The results in this study significantly modify the sorption of metal ions in aqueous solution. The experimental data was found to obey the pseudo-second-order kinetic model, and the adsorption isotherms data of Ni(II) ions on the MGO were fit well by the Langmuir isotherm model. The thermodynamic results illustrated that the adsorption process was endothermic and spontaneous in nature. The adsorption of Ni(II) on MGO is strongly dependent on pH values which increases with pH increasing from 2.0 to 9.0, and then maintains high level. This research indicates that MGO has many advantages such as easy magnetic separation, excellent repeatability and environment-friend, it has a good application prospect as an effective sorbent for the simple and rapid removal of Ni(II) and related metal ions pollutants from water samples.

Acknowledgement

Financial supports from the National Natural Science Foundation of China (51372199) and the research project of department of education of Zhejiang province (Y201431557) are acknowledged.

References

[1] J.O. Nriagu, J.M. Pacyna, Quantitative assessment of worldwide contamination of air, water and soils by trace metals, Nature, 333 (1988) 134–139.
[2] G. Sheng, A. Alsaedi, W. Shammakh, S. Monaquel, J. Sheng, X. Wang, H. Li, Y. Huang, Enhanced sequestration of selenite in water by nanoscale zero valent iron immobilization on carbon nanotubes by a combined batch, XPS and XAFS investigation, Carbon, 99 (2016) 123–130.
[3] G. Sheng, Y. Tang, W. Linghu, L. Wang, J. Li, H. Li, X. Wang, Y. Huang, Enhanced immobilization of ReO^{4-} by nanoscale zerovalent iron supported on layered double hydroxide via an advanced XAFS approach: Implications for TcO^{4-} sequestration, Appl. Catal. B Environ., 192 (2016) 268–276.
[4] B. Hu, W. Cheng, H. Zhang, G. Sheng, Sorption of radionickel to goethite: effect of water quality parameters and temperature, J. Radioanal. Nucl. Chem., 285 (2010) 389–398.
[5] G. Sheng, B. Hu, Role of solution chemistry on the trapping of radionuclide Th(VI) using titanate nanotubes as an efficient adsorbent, J. Radioanal. Nucl. Chem., 298 (2013) 455–464.
[6] G. Sheng, X. Shao, Y. Li, J. Li, H. Dong, W. Cheng, X. Gao, Y. Huang, Enhanced removal of U(VI) by nanoscale zerovalent iron supported on Na-bentonite and an investigation of mechanism, J. Phys. Chem. A, 118 (2014) 2952–2958.
[7] D. Zhao, X. Wang, S. Yang, Z. Guo, G. Sheng, Impact of water quality parameters on the sorption of U(VI) onto hematite, J. Environ. Radioactiv., 103 (2012) 20–29.
[8] G. Sheng, H. Dong, Y. Li, Characterization of diatomite and its application for the retention of radiocobalt: role of environmental parameters, J. Environ. Radioactiv., 113 (2012) 108–115.
[9] B. Hu, F. Ye, X. Ren, D. Zhao, G. Sheng, H. Li, J. Ma, X. Wang, Y. Huang, X-ray absorption fine structure study of enhanced sequestration of U(VI) and Se(IV) by montmorillonite decorated zero-valent iron nanoparticles, Environ. Sci. Nano., 3 (2016) 1460–1472.
[10] Y. Zou, X. Wang, A. Khan, P. Wang, Y. Liu, A. Alsaedi, T. Hayat, X. Wang, Environmental remediation and application of nanoscale zero-valent iron and its composites for the removal of heavy metal ions: a review, Environ. Sci. Technol., 50 (2016) 7290–7304.
[11] S. Yu, X. Wang, Z. Chen, J. Wang, S. Wang, T. Hayat, X. Wang, Layered double hydroxide intercalated with aromatic acid anions for the efficient capture of aniline from aqueous solution, J. Hazard. Mater., 321 (2016) 111–120.
[12] G. Sheng, P. Yang, Y. Tang, Q. Hu, H. Li, X. Ren, B. Hu, X. Wang, Y. Huang, New insights into the primary roles of diatomite in the enhanced sequestration of UO_2^{2+} by zerovalent iron nanoparticles: An advanced approach utilizing XPS and EXAFS, Appl. Catal. B Environ., 193 (2016) 189–197.
[13] X. Ren, S. Yang, F. Hu, B. He, J. Xu, X. Tan, X. Wang, Microscopic level investigation of Ni(II) sorption on Na-rectorite by EXAFS technique combined with statistical F-tests, J. Hazard. Mater., 252–253 (2013) 2–10.
[14] X. Wang, J. Huang, H. Hu, J. Wang, Y. Qin, Determination of kinetic and equilibrium parameters of the batch adsorption of Ni(II) from aqueous solutions by Na-mordenite, J. Hazard. Mater., 142 (2007) 468–476.
[15] P. Panneerselvam, N. Morad, K.A. Tan, Magnetic nanoparticle (Fe_3O_4) impregnated onto tea waste for the removal of nickel(II) from aqueous solution, J. Hazard. Mater., 186 (2011) 160–168.
[16] U. Garg, M. Kaur, V. Garg, D. Sud, Removal of Ni(II) from aqueous solution by adsorption on agriculture waste biomass using a response surface methodological approach, Bioresour. Technol., 99 (2008) 1325–1331.
[17] S. Pacheo, M. Medina, F. Valencia, J. Tapia, Removal of inorganic mercury from polluted water using structured nanoparticles, J. Environ. Eng., 132 (2006) 342–349.
[18] Y. Ren, N. Yan, Q. Wen, Z. Fan, T. Wei, M. Zhang, J. Ma, Graphene/δ-MnO_2 composite as adsorbent for the removal of nickel ions from wastewater, Chem. Eng. J., 175 (2011) 1–7.
[19] G. Sheng, R. Shen, H. Dong, Y. Li, Colloidal diatomite, radionickel and humic substance interaction: A combined batch, XPS and EXAFS investigation, Environ. Sci. Pollut. Res., 20 (2013) 3708–3717.
[20] G. Sheng, S. Yang, J. Sheng, J. Hu, X. Tan, X. Wang, Macroscopic and microscopic investigation of Ni(II) sequestration on diatomite by batch, XPS and EXAFS techniques, Environ. Sci. Technol., 45 (2011) 7718–7726.
[21] S. Yang, G. Sheng, Z. Guo, X. Tan, J. Xu, X. Wang, Investigation of radionuclide ^{63}Ni(II) sequestration mechanisms on mordenite by batch and EXAFS spectroscopy study, Sci. China. Chem., 55 (2012) 632–642.
[22] Q. Fan, D. Shao, Y. Lu, W. Wu, X. Wang, Effect of pH, ionic strength, temperature and humic substances on the sorption of Ni(II) to Na-attapulgite, Chem. Eng. J., 150 (2009) 188–195.
[23] X. Tan, C. Chen, S. Yu, X. Wang, Sorption of Ni^{2+} on Na-rectorite studied by batch and spectroscopy methods, Appl. Geochem., 23 (2008) 2767–2777.
[24] S. Yang, J. Li, Y. Lu, Y. Chen, X. Wang, Sorption of Ni(II) on GMZ bentonite: effects of pH, ionic strength, foreign ions, humic acid and temperature, Appl. Radiat. Isot., 67 (2009) 1600–1608.
[25] G. Sheng, L. Ye, Y. Li, H. Dong, H. Li, X. Gao, Y. Huang, EXAFS study of the interfacial interaction of nickel(II) on titanate nanotubes: Role of contact time, pH and humic substances, Chem. Eng. J., 248 (2014) 71–78.

[26] S. Yang, J. Li, D. Shao, J. Hu, X. Wang, Adsorption of Ni(II) on oxidized multi-walled carbon nanotubes: effect of contact time, pH, foreign ions and PAA, J. Hazard. Mater., 166 (2009) 109–116.
[27] G. Sheng, Y. Li, X. Yang, X. Ren, S. Yang, J. Hu, X. Wang, Efficient removal of arsenate by a versatile magnetic graphene oxide composites, RSC Adv., 2 (2012) 12400–12407.
[28] Y. Li, G. Sheng, J. Sheng, Magnetite decorated graphene oxide for the highly efficient immobilization of Eu(III) from aqueous solution, J. Mol. Liq., 199 (2014) 474–480.
[29] X. Wang, Z. Chen, X. Wang, Graphene oxides for simultaneous highly efficient removal of trace level radionuclides from aqueous solutions, Sci. China Chem., 58 (2015) 1766–1773.
[30] X. Wang, Q. Fan, Z. Chen, Q. Wang, J. Li, A. Hobiny, A. Alsaedi, X. Wang, Surface modification of graphene oxides by plasma techniques and their application for environmental pollution cleanup, Chem. Rec., 16 (2016) 295–318.
[31] Y. Zou, X. Wang, Z. Chen, W. Yao, Y. Ai, Y. Liu, T. Hayat, A. Alsaedi, N. Alharbi, X. Wang, Superior coagulation of graphene oxides on nanoscale layered double hydroxides and layered double oxides, Environ. Pollut., 219 (2016) 107–117.
[32] S. Yu, X. Wang, Y. Ai, X. Tan, T. Hayat, W. Hu, X. Wang, Experimental and theoretical studies on competitive adsorption of aromatic compounds on reduced graphene oxides, J. Mater. Chem. A, 4 (2016) 5654–5662.
[33] S. Yu, X. Wang, X. Tan, X. Wang, Sorption of radionuclides from aqueous systems onto graphene oxide-based materials: a review, Chem Inform., 46 (2015) 593–612.
[34] S. Yu, X. Wang, Y. Ai, Y. Liang, Y. Ji, J. Li, T. Hayat, A. Alsaedi, X. Wang, Spectroscopic and theoretical study on the counterion effect of Cu(II) ions and graphene oxide interaction with titanium dioxide, Environ. Sci. Nano., 3 (2016) 1361–1368.
[35] X. Wang, Q. Fan, S. Yu, Z. Chen, Y. Ai, Y. Sun, A. Hobiny, A. Alsaedi, X. Wang, High sorption of U(VI) on graphene oxides studied by batch experimental and theoretical calculations, Chem. Eng. J., 287 (2016) 448–455.
[36] H. Chen, B. Gao, H. Li, Removal of sulfamethoxazole and ciprofloxacin from aqueous solutions by graphene oxide, J. Hazard. Mater., 282 (2015) 201–207.
[37] J. Wang, Z. Chen, B. Chen, Adsorption of polycyclic aromatic hydrocarbons by graphene and graphene oxide nanosheets, Environ. Sci. Technol., 48 (2014) 4817–4825.
[38] J. Li, C. Chen, R. Zhang, X. Wang, Reductive immobilization of Re(VII) by graphene modified nanoscale zero-valent iron particles using a plasma technique, Sci. China Chem., 59 (2016) 150–158.
[39] D. Zhao, X. Gao, C. Wu, R. Xie, S. Feng, C. Chen, Facile preparation of amino functionalized graphene oxide decorated with Fe_3O_4 nanoparticles for the adsorption of Cr(VI), Appl. Surf. Sci., 384 (2016) 1–9.
[40] X. Deng, L. Lü, H. Li, F. Luo, The adsorption properties of Pb(II) and Cd(II) on functionalized graphene prepared by electrolysis method, J. Hazard. Mater., 183 (2010) 923–930.
[41] J. Li, C. Chen, K. Zhu, X. Wang, Nanoscale zero-valent iron particles modified on reduced graphene oxides using a plasma technique for Cd(II) removal, J. Taiwan Inst. Chem. E, 59 (2015) 389–394.
[42] X. Li, M. Yu, Q. Lv, Y. Tan, Sequestration of Ni(II) onto graphene oxide from synthetic wastewater as affected by coexisting constituents, Desal. Water Treat., 57 (2016) 20904–20914.
[43] X. Li, Y. Fang, X. Tang, Using graphene oxide as a superior adsorbent for the highly efficient immobilization of Cu(II) from aqueous solution, J. Mol. Liq., 199 (2014) 237–243.
[44] J. Li, S. Zhang, C. Chen, G. Zhao, X. Yang, J. Li, X. Wang, Removal of Cu(II) and fulvic acid by graphene oxide nanosheets decorated with Fe_3O_4 nanoparticles, ACS. Appl. Mater. Inter., 4 (2012) 4991–5000.
[45] G. Sheng, S. Yang, Y. Li, X. Gao, Y. Huang, X. Wang, Retention mechanisms and microstructure of Eu(III) on manganese dioxide studied by batch and high resolution EXAFS technique, Radiochim. Acta., 102 (2014) 155–167.
[46] G. Sheng, J. Hu, H. Li, J. Li, Y. Huang, Enhanced sequestration of Cr(VI) by nanoscale zero-valent iron supported on layered double hydroxide by batch and XAFS study, Chemosphere, 148 (2016) 227–232.
[47] G. Sheng, W. Linghu, Z. Chen, D. Xu, A. Alsaedi, W. Shammakh, S. Monaquel, J. Sheng, Sequestration of selenate and selenite onto titanate nanotube: A combined classical batch and advanced EXAFS approach, Environ. Nano. Monit. Manage., 6 (2016) 152–158.
[48] G. Sheng, H. Dong, R. Shen, Y. Li, Microscopic insights into the temperature-dependent adsorption of Eu(III) onto titanate nanotubes studied by FTIR, XPS, XAFS and batch technique, Chem. Eng. J., 217 (2013) 486–494.
[49] G. Sheng, S. Yang, D. Zhao, J. Sheng, X. Wang, Adsorption of Eu(III) on titanate nanotubes studied by a combination of batch and EXAFS technique, Sci. China Chem., 55 (2012) 182–194.
[50] F. Zhang, Y. Song, S. Song, R. Zhang, W. Hou, Synthesis of magnetite-graphene oxide-layered double hydroxide composites and applications for the removal of Pb(II) and 2,4-dichlorophenoxyacetic acid from aqueous solutions, ACS Appl. Mater. Interfaces, 7 (2015) 7251–7263.
[51] C. Zhu, S. Guo, Y. Fang, S. Dong, Reducing sugar: New functional molecules for the green synthesis of graphene nanosheets, ACS Nano., 4 (2010) 2429–2437.
[52] X. Yang, C. Chen, J. Li, G. Zhao, X. Ren, X. Wang, Graphene oxide-iron oxide and reduced graphene oxide-iron oxide hybrid materials for the removal of organic and inorganic pollutants, RSC Adv., 2 (2012) 8821–8826.
[53] Y. Sun, D. Shao, C. Chen, S. Yang, X. Wang, Highly efficient enrichment of radionuclides on graphene oxide-supported polyaniline, Environ. Sci. Technol., 47 (2013) 9904–9910.
[54] J. Zou, H. Liu, J. Luo, Q. Xing, H. Du, X. Jiang, X. Luo, S. Luo, S. Suib, Three-dimensional reduced graphene oxide coupled with Mn_3O_4 for highly efficient removal of Sb(III) and Sb(V) from water, ACS Appl. Mater. Inter., 8 (2016) 18140–18149.
[55] Y. Sharma, V. Srivastava, A. Mukherjee, Synthesis and application of nano-Al_2O_3 powder for the reclamation of hexavalent chromium from aqueous solutions, J. Chem. Eng. Data., 55 (2010) 2390–2398.
[56] F. Fang, L. Konga, J. Huang, S. Wua, K. Zhang, X. Wang, B. Sun, Z. Jin, J. Wang, X. Huang, J. Liu, Removal of cobalt ions from aqueous solution by an amination graphene oxide nanocomposite, J. Hazard. Mater., 270 (2014) 1–10.
[57] G. Sheng, Y. Li, H. Dong, D. Shao, Environmental condition effects on radionuclide ^{64}Cu(II) sequestration to a novel composite: Polyaniline grafted multiwalled carbon nanotubes, J. Radioanal. Nucl. Ch., 293 (2012) 797–806.
[58] Z. Wang, B. Yue, J. Teng, F. Jiao, X. Jiang, J. Yu, X. Chen, Tartaric acid modified graphene oxide as a novel adsorbent for high-efficiently removal of Cu(II) and Pb(II) from aqueous solutions, J. Taiwan Inst. Chem. E, 66 (2016) 181–190.
[59] Y. Zou, X. Wang, Y. Ai, Y. Liu, Y. Ji, H. Wang, T. Hayat, A. Alsaedi, W. Hu, X. Wang, β-cyclodextrin modified graphitic carbon nitride for the removal of pollutants from aqueous solution: experimental and theoretical calculation study, J. Mater. Chem. A, 4 (2016) 14170–14179.
[60] S. Yu, X. Wang, Z. Chen, X. Tan, H. Wang, J. Hu, A. Alsaedi, N. Alharbi, W. Guo, X. Wang, Interaction mechanism of radionickel on Na-montmorillonite: Influences of pH, electrolyte cations, humic acid and temperature, Chem. Eng. J., 302 (2016) 77–85.
[61] W. Yao, X. Wang, Y. Liang, S. Yu, P. Gu, Y. Sun, C. Xu, J. Chen, T. Hayat, A. Alsaedi, X. Wang, Synthesis of novel flower-like layered double oxides/carbon dots nanocomposites for U(VI) and ^{241}Am(III) efficient removal: batch and EXAFS studies, Chem. Eng. J., 332 (2018) 775–786.
[62] S. Yu, X. Wang, H. Pang, R. Zhang, W. Song, D. Fu, T. Hayat, X. Wang, Boron nitride-based materials for the removal of pollutants from aqueous solutions: a review, Chem. Eng. J., 333 (2018) 343–360.
[63] J. Wang, P. Wang, H. Wang, J. Dong, W., Chen, X. Wang, S. Wang, T. Hayat, A. Alsaedi, X. Wang, Preparation of molybdenum disulfide coated Mg/Al layered double hydroxide composites for efficient removal of chromium(VI), ACS Sustain. Chem. Eng., 5 (2017) 5550–5561.

[64] X. Wang, Z. Chen, Y. Liang, D. Jia, W. Chen, Z. Cui, X. Wang, Layered silicate RUB-15 for efficient removal of UO_2^{2+} and heavy metal ions by ion-exchange, Environ. Sci-Nano., 4 (2017) 1851–1858.
[65] S. Yu, X. Wang, S. Yang, G. Sheng, A. Alsaedi, T. Hayat, X. Wang, Interaction of radionuclides with natural and manmade materials using XAFS technique, Sci. China Chem., 60 (2017) 170–187.
[66] S. Yu, J. Wang, S. Song, K. Sun, J. Li, X. Wang, Z. Chen, X. Wang, One-pot synthesis of graphene oxide and Ni-Al layered double hydroxides nanocomposites for the efficient removal of U(VI) from wastewater, Sci. China Chem., 60 (2017) 415–422.
[67] G.Z. Kyzas, N.A. Travlou, E.A. Deliyanni, The role of chitosan as nanofiller of graphite oxide for the removal of toxic mercury ions, Colloids Surfaces B: Biointerfaces, 113 (2014) 467–476.
[68] G.Z. Kyzas, Z. Terzopoulou, V. Nikolaidis, E. Alexopoulou, D.N. Bikiaris, Low-cost hemp biomaterials for nickel ions removal from aqueous solutions. J. Molec. Liq., 209 (2015) 209–218.

Supporting information

Characterization of MGO

The typical scanning electron microscope (SEM) and transmission electron microscope (TEM) images of GO and MGO are shown in Fig. S1A–D. As seen from Fig. S1A, GO exhibited layered structure with smooth surface and many wrinkles, it was observed that many nanoparticles were homogeneously anchored onto the rough surface of the graphene oxide sheets for MGO (Fig. S1B). More finely, the TEM image (Fig. S1C and D) shows that the GO film is transparent and Fe_3O_4 nanoparticles are well dispersed on the surface which suggest that MGO nanocomposites are formed. The elemental composition analysis illustrated that the oxygen percentage of GO and MGO were as high as –55.3% (Fig. S1E) and –49.7% (Fig. S1F), indicating sufficient oxidation of graphite during synthesis process using modified Hummers' method. Most importantly, the Fe could be determined content in MGO was –11.5%, which is ideal. Besides, a small amount of sulfur was found, which is likely due to the usage of H_2SO_4 during oxidation process.

To obtain the structural information about samples, X-ray diffraction (XRD) characterization was conducted. Fig. S2A shows the XRD patterns of the prepared GO and MGO, displaying that the intense diffraction peaks indexed to (220), (311), (400), (422), (511), and (440) planes appearing at 2θ = 30.11°, 35.59°, 43.46°, 53.76°, 57.36°, and 62.78°, respectively, are consistent with the standard XRD data for the cubic phase Fe_3O_4 with a face-centered cubic (fcc) structure and indicating the existence of Fe_3O_4 nanoparticles in the as-obtained MGO composite [50]. Interestingly, the characteristic peak of GO located at 8.42° disappeared, confirming the formation of graphene [51]. Fourier transform infrared spectroscopy (FTIR) spectra were also measured to characterize the GO and MGO are shown Fig. S2B. The strong and wide peaks at 3383 cm^{-1} were assigned to the stretching vibration of the –OH band of H_2O. The other characteristic peaks of C–O (–1072 cm^{-1}), C=O (–1377 cm^{-1}), C=C (–1628 cm^{-1}), and COOH (–1731 cm^{-1}) can be observed. The FTIR spectrum of MGO showed significant differences from that of GO. There was displacement and change in the intensities of the characteristic absorption bands of oxygen functionalities. Most of all it can be clearly seen that the peak around –576 cm^{-1}, which is attributed to Fe–O, is not present in the FTIR spectrum of the GO [3]. According to the Raman spectra of the GO and MGO in Fig.S2C, the obvious peaks at –1236 cm^{-1} and –1469 cm^{-1} of GO, –1223 cm^{-1} and –1454 cm^{-1}, which can be attributed to the disordered structure (D band, sp^3 carbon atoms of disorders and defects) and graphite structure (G band, sp^2 carbon atoms in graphitic sheets) of GO, respectively [4]. Comparing with GO, the D and G peaks of MGO occur raman shifts and damping

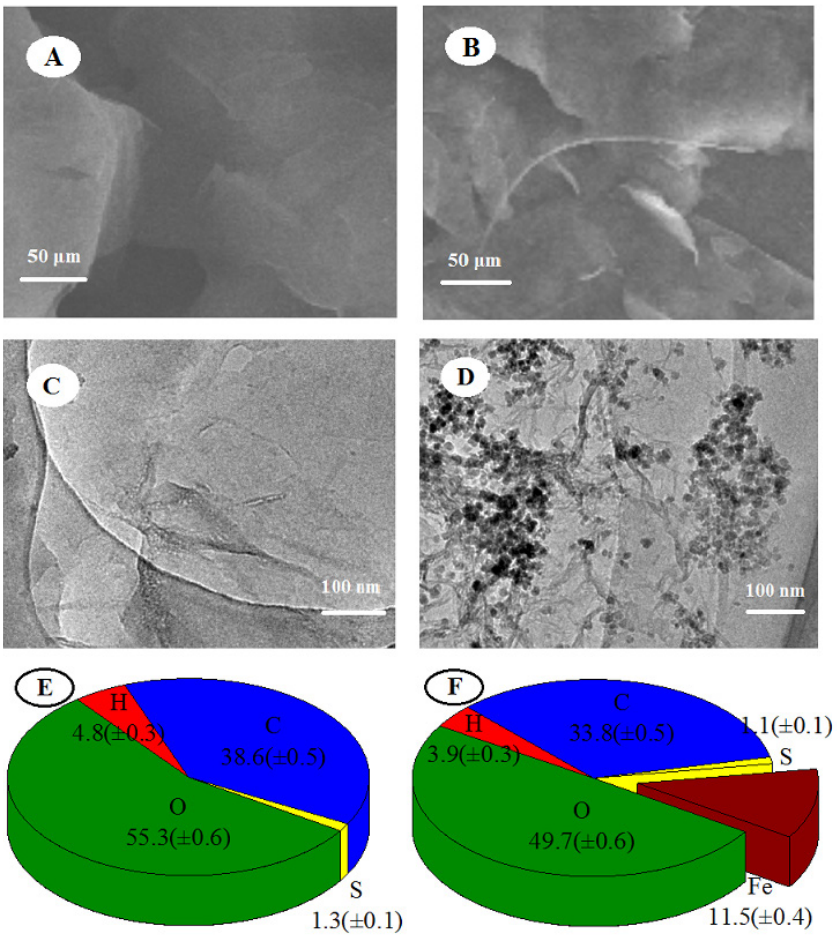

Fig. S1. SEM images of GO (A) and MGO (B), TEM images of GO (C) and MGO (D), and Elemental composition analysis of GO (E) and MGO (F). = 0.1 mol·L^{-1} $NaNO_3$.

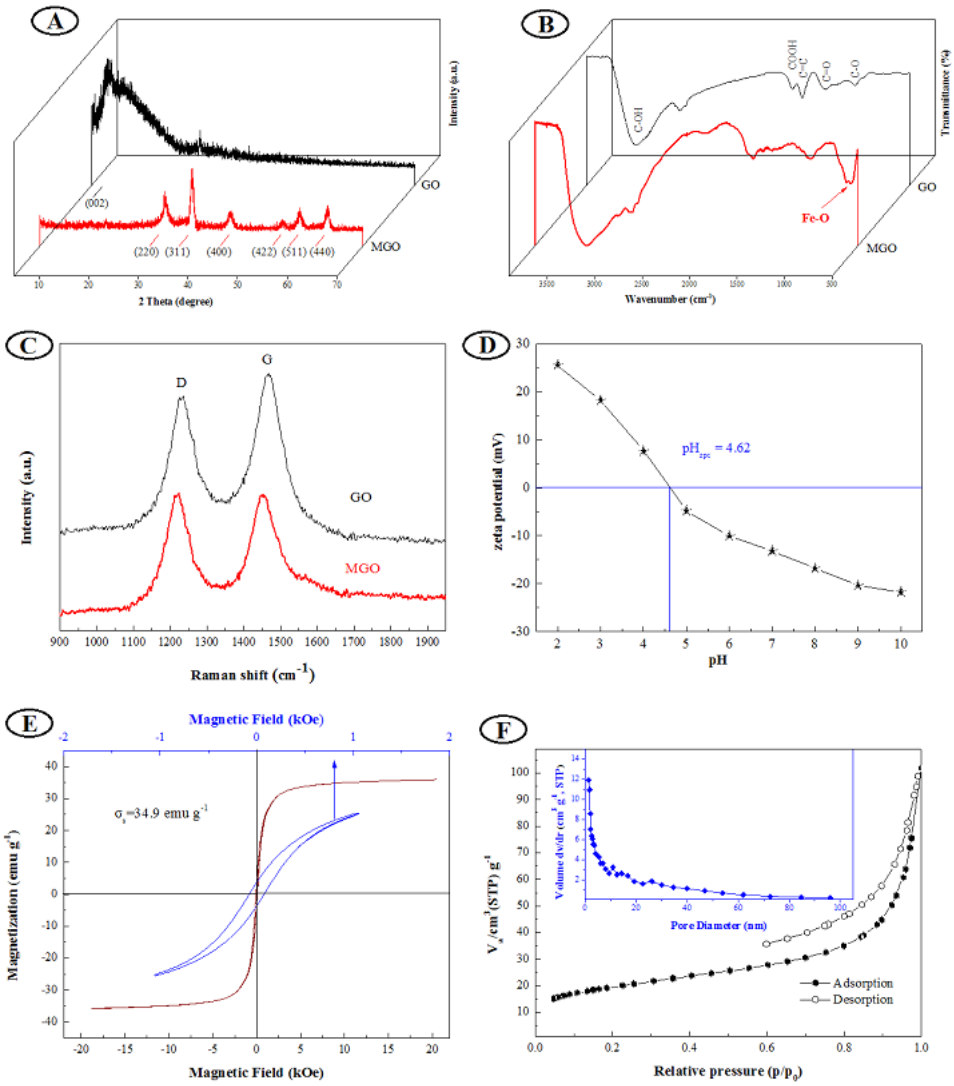

Fig. S2. (A) XRD patterns of GO and MGO, (B) FTIR spectra of GO and MGO, (C) Raman spectra of GO and MGO, and Zeta potential (D), Magnetic hysteresis loop (E), BET pattern and particles size distribution (F) of the MGO composites.

which provide evidence for the charge transfer between GO and Fe_3O_4, and shows a strong interaction between GO and Fe_3O_4. Fig. S2D shows the zeta potentials of the MGO at different pH conditions. The value of the zeta potentials (pH_{zpc}) was calculated to be zero at pH 4.62, and the zeta potential becomes negative with the increase of pH. The magnetization property of MGO was investigated at room temperature by measuring the magnetization curve (Fig. S2E). The saturation magnetization (Ms) of MGO was 34.9 emu g^{-1} (magnetic field ±20 kOe), suggesting that MGO had a high magnetism and can be easily removed from aqueous solutions by magnetic material such as magnet. In addition, BET (Fig. S2F) results show the specific surface area of MGO is 39.77 m^2 g^{-1} and the micropore volume of MGO is 0.13 cm^3 g^{-1}. The large surface area and mesoporous structure of the MGO composite not only provide much more reaction sites to make the sufficient contact between the adsorbent and adsorbate but also prevent the leaching and agglomeration of MGO nanoparticles [5].

References

[1] F. Zhang, Y. Song, S. Song, R. Zhang, W. Hou, Synthesis of magnetite-graphene oxide-layered double hydroxide composites and applications for the removal of Pb(II) and 2,4-dichlorophenoxyacetic acid from aqueous solutions, ACS Appl. Mater. Interfaces, 7 (2015) 7251–7263.

[2] C. Zhu, S. Guo, Y. Fang, S. Dong, Reducing sugar: New functional molecules for the green synthesis of grapheme nanosheets, ACS Nano., 4 (2010) 2429–2437.

[3] X. Yang, C. Chen, J. Li, G. Zhao, X. Ren, X. Wang, Graphene oxide-iron oxide and reduced graphene oxide-iron oxide hybrid materials for the removal of organic and inorganic pollutants, RSC. Advances., 2 (2012) 8821–8826.

[4] Y. Sun, D. Shao, C. Chen, S. Yang, X. Wang, Highly efficient enrichment of radionuclides on graphene oxide-supported polyaniline, Environ. Sci. Technol. 47 (2013) 9904–9910.

[5] J. Zou, H. Liu, J. Luo, Q. Xing, H. Du, X. Jiang, X. Luo, S. Luo, S. Suib, Three-dimensional reduced graphene oxide coupled with Mn_3O_4 for highly efficient removal of Sb(iii) and Sb(v) from water, ACS Appl. Mater. Inter., 8 (2016) 18140–18149.